Electronic Supplementary Information (ESI †)

Nonionic Oligo(ethylene glycol)-substituted Viologen Negolytes for Aqueous Organic Redox Flow Batteries

*Yanxin Yao[a], Wanzhen Ma[b], Jiafeng Lei[a], Zengyue Wang[a], Yi-Chun Lu[*a] and Lei Liu[*b]*

a. Electrochemical Energy and Interfaces Laboratory, Department of Mechanical and Automation Engineering, The Chinese University of Hong Kong, Shatin, N.T. 999077, Hong Kong SAR, China. E-mail: yichunlu@mae.cuhk.edu.hk

b. College of Chemistry and Materials Science, Anhui Normal University, Wuhu 241000, China. E-mail: liulei@ahnu.edu.cn

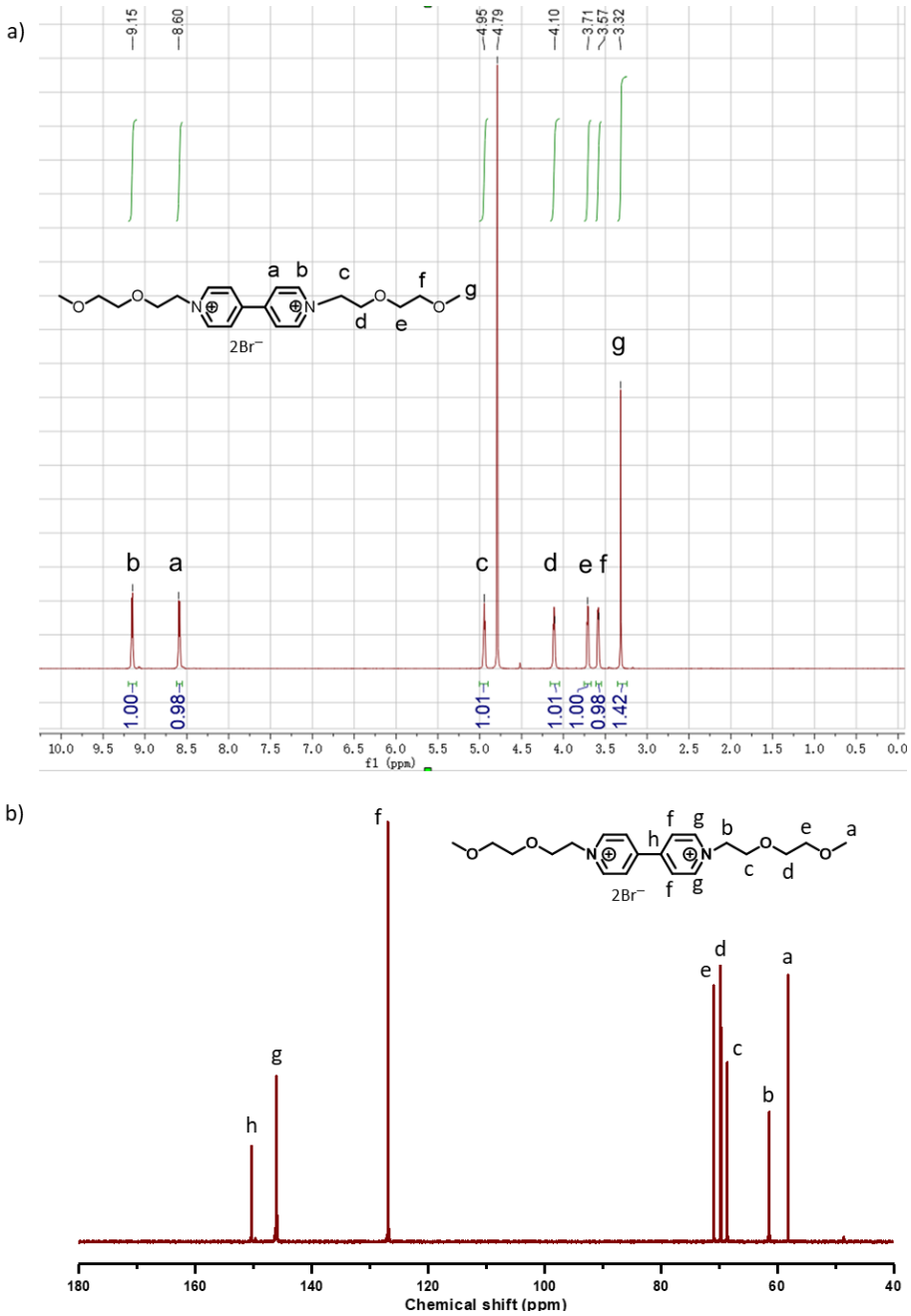

Fig. S1 ^{1}H NMR (a) and ^{13}C NMR (b) spectra of Vi-OEG2 in D_2O.

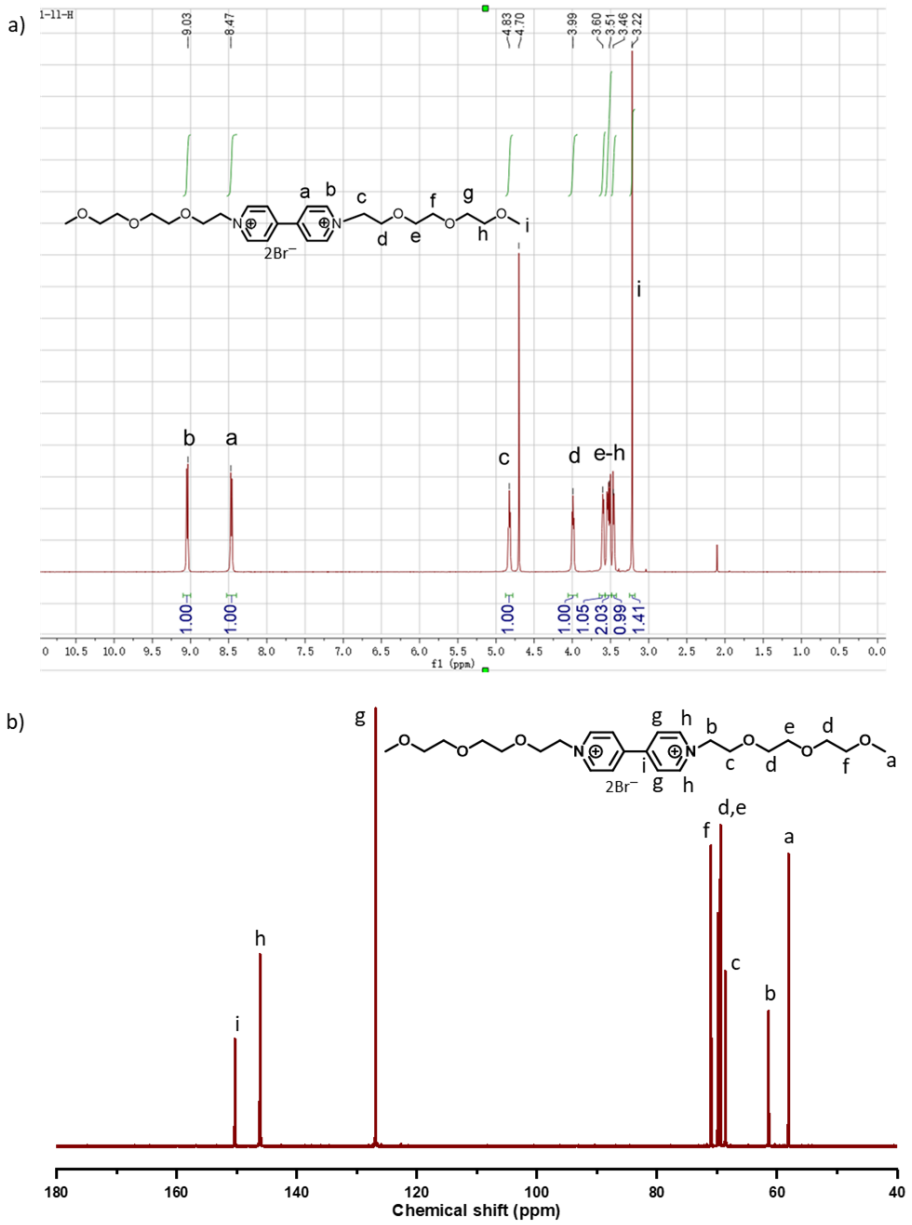

Fig. S2 ^{1}H NMR (a) and ^{13}C NMR (b) spectra of Vi-OEG3 in D_2O.

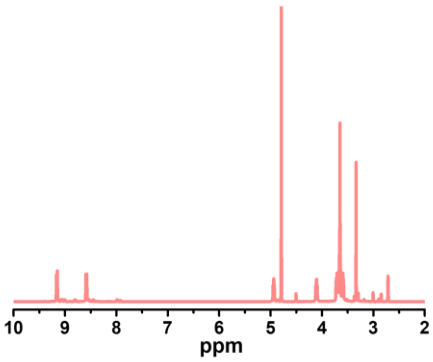

Fig. S3 ^{1}H NMR of Vi-OEG4.

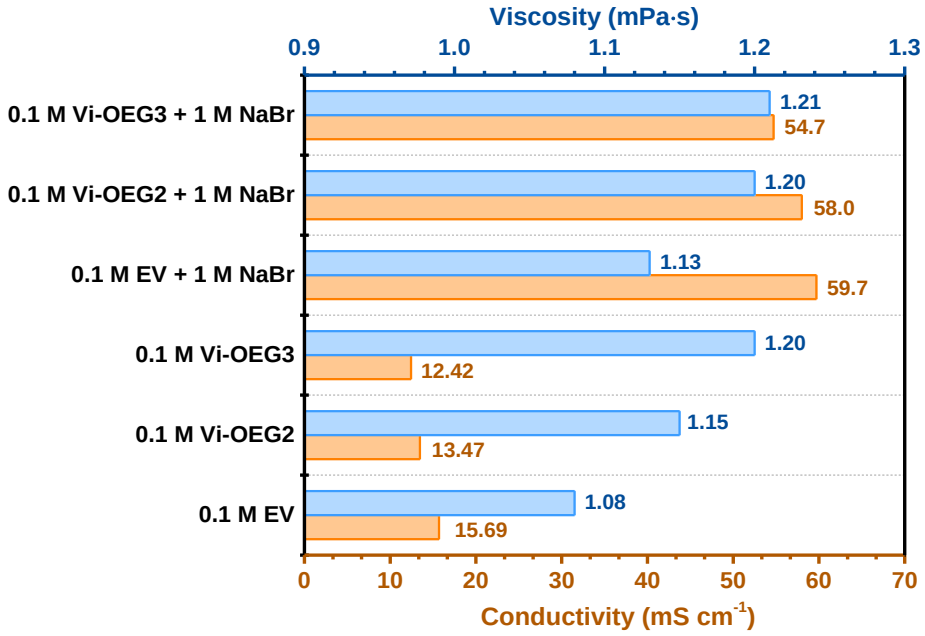

Fig. S4 Conductivity and viscosity measurement of 0.1 M EV, Vi-OEG2 and Vi-OEG3 with and without 1 M NaBr.

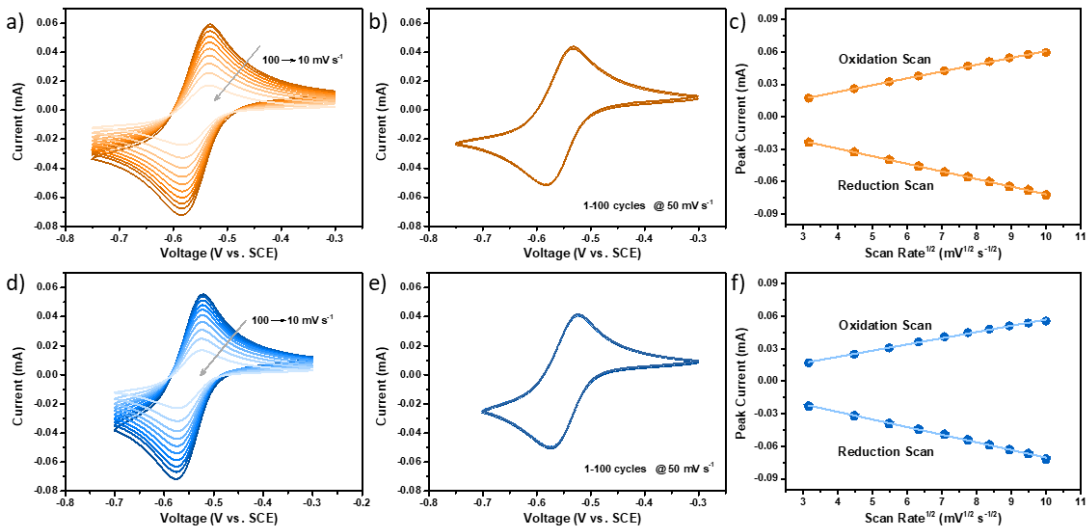

Fig. S5 CV curves of (a) Vi-OEG2 and (d) Vi-OEG3 at different scanning rates from 10 to 100 mV s^{-1}. CV curves of (b) Vi-OEG2 and (e)Vi-OEG3 at the 1st, 10th, 20th, ……, 90th, and 100th cycles at 50 mV s^{-1}. Linearly increased peak currents with the increased square root of scanning rates of (c) Vi-OEG2 and (f)Vi-OEG3. Solution: 5 mM Vi-OEG2 or Vi-OEG3 in 0.5 M NaBr.

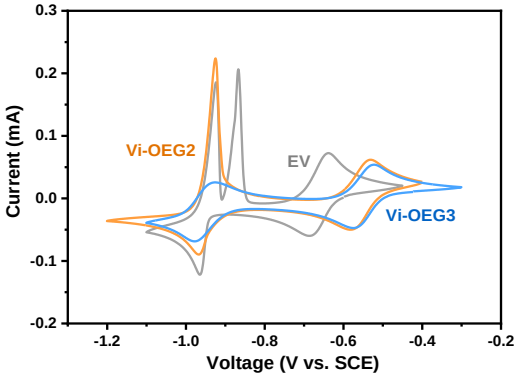

Fig. S6 Cyclic voltammograms of EV, Vi-OEG2, and Vi-OEG3. Condition: 5 mM viologens in 0.5 M NaBr aqueous electrolyte at a scan rate of 50 mV s^{-1}.

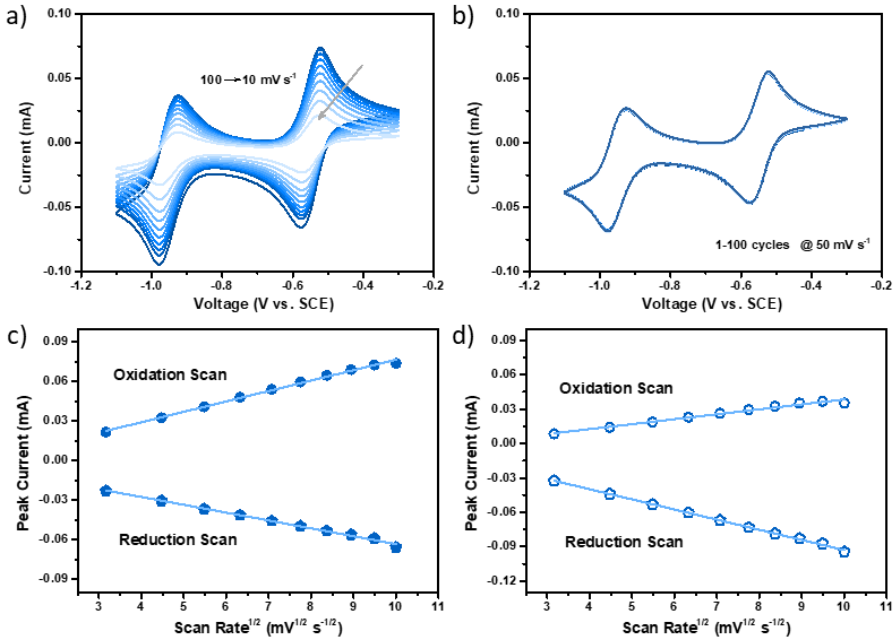

Fig. S7 (a) CV curves of Vi-OEG3 at different scanning rates from 10 to 100 mV s^{-1}. (b) CV curves of Vi-OEG3 at the 1st, 10th, 20th, ……, 90th, and 100th cycles at 50 mV s^{-1}. Linearly increased peak currents with the increased square root of scanning rates of (c) the first-electron reduction and (d) the second-electron reduction of Vi-OEG3. Solution: 5 mM Vi-OEG3 in 0.5 M NaBr.

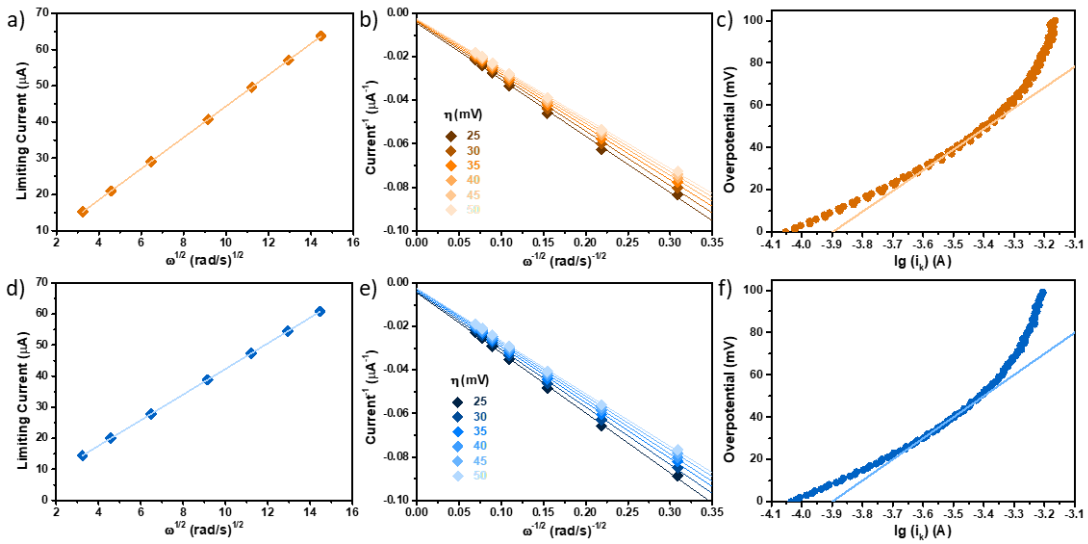

Fig. S8 Levich plots of the limiting current vs. the square root of rotation rates for (a) Vi-OEG2 and (d) Vi-OEG3. Koutecký-Levich plot (i^{-1} vs. $\omega^{-1/2}$) of (b) Vi-OEG2 and (e) Vi-OEG3. The current response, i^{-1}, is shown for different reduction overpotentials η (η = 25, 30, 35, 40, 45, and 50 mV). The plots of overpotentials over the logarithm of kinetic current and the corresponding fitted Tafel plot for (c) Vi-OEG2 and (f) Vi-OEG3. Condition: 1.0 mM Vi-OEG2 or Vi-OEG3 in 0.5 M NaCl at a scan rate of 5 mV s^{-1}.

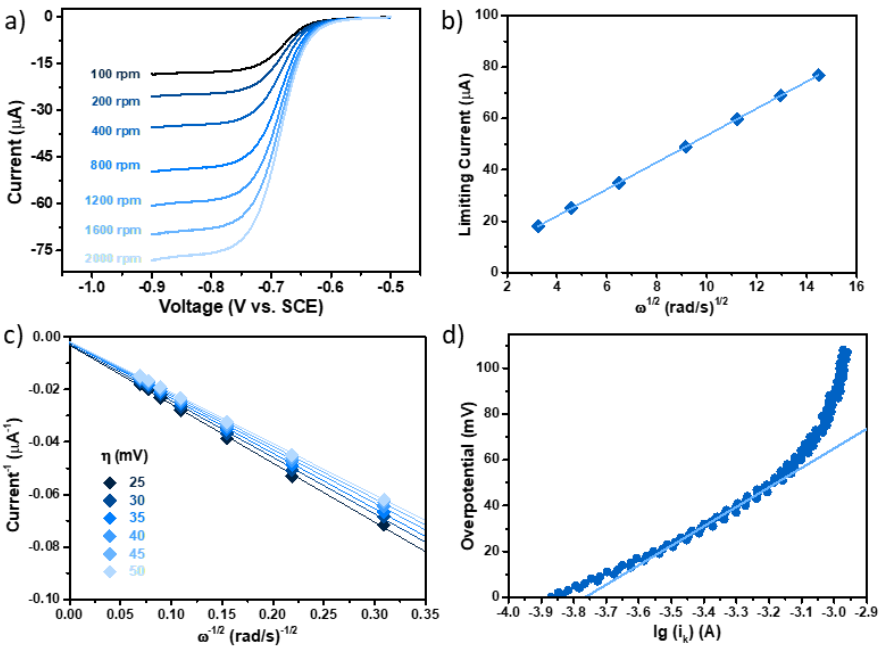

Fig. S9 (a) Linear sweep voltammograms of EV. (b) Levich plots of the limiting current vs. the square root of rotation rates for EV. (c) Koutecký-Levich plot (i^{-1} vs. $\omega^{-1/2}$) of EV. The current response, i^{-1}, is shown for different reduction overpotentials η (η = 25, 30, 35, 40, 45, and 50 mV). (d) The plots of overpotentials over the logarithm of kinetic current and the corresponding fitted Tafel plot for EV. Condition: 1.0 mM EV in 0.5 M NaCl at a scan rate of 5 mV s^{-1}.

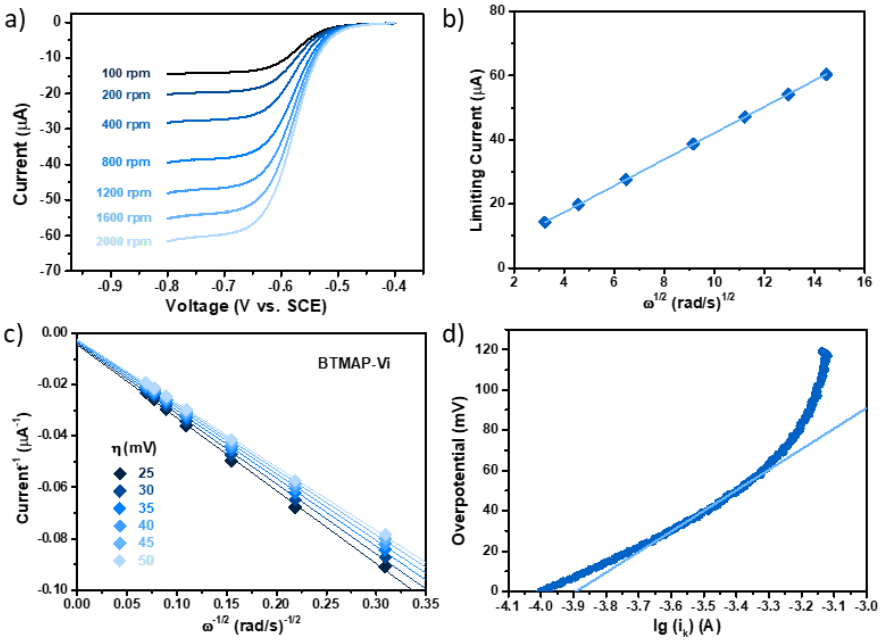

Fig. S10 (a) Linear sweep voltammograms of BTMAP-Vi. (b) Levich plots of the limiting current vs. the square root of rotation rates for BTMAP-Vi. (c) Koutecký-Levich plot (i^{-1} vs. $\omega^{-1/2}$) of BTMAP-Vi. The current response, i^{-1}, is shown for different reduction overpotentials η (η = 25, 30, 35, 40, 45, and 50 mV). (d) The plots of overpotentials over the logarithm of kinetic current and the corresponding fitted Tafel plot for BTMAP-Vi. Condition: 1.0 mM BTMAP-Vi in 0.5 M NaCl at a scan rate of 5 mV s^{-1}.

RRDE was further exploited to understand the redox processes of EV and Vi-OEG3. The disk and ring currents were recorded by negatively stepping the disk potential within a similar potential range to their CVs while holding the ring current at a positive potential to ensure that viologens are continuously oxidized. For EV, shown in **Fig. S11**, two diffusion-limiting disk current plateaus were observed during the negative-going scan. The first diffusion-limiting ring current plateau can be attributed to the reversible oxidation of $EV^{\bullet+}$ to EV^{2+}, consistent with the CV results. The ring current started to decrease as soon as the disk potential entered the second plateau and dropped to zero at the end of the second disk-limiting current (100 rpm). Noted that at higher rotation rates, the solid EV^0 could be potentially thrown to the ring, resulting in weak ring currents. During the positive-going scan, after the disk potential entered the first plateau potential, $EV^{\bullet+}$ was generated from both the oxidation of deposited EV^0 and the reduction of EV^{2+}, and thus the flux of $EV^{\bullet+}$ arriving at the ring increased. It should be noted that the oxidation currents of both disk and ring electrodes show two peaks at − 0.93 V vs. SCE and − 0.86 V vs. SCE at higher rotation rates (400 − 2000 rpm), which is consistent with the CV curves. This observation indicates that the reduction product of the second disk reaction (EV^0) cannot be oxidized on the ring (insoluble) (**Fig. S11a**). In contrast, for Vi-OEG3 (**Fig. S12**), there were two diffusion-limiting current plateaus for both disk and ring during negative/positive-going scans, which suggests no passivation phenomenon during the two-electron redox reaction of Vi-OEG3. Thus, the RRDE experiment revealed that the second-electron redox reaction of Vi-OEG3 exhibits fast kinetics with high reversibility, which strongly contrasts with that of EV with passivation features.[1]

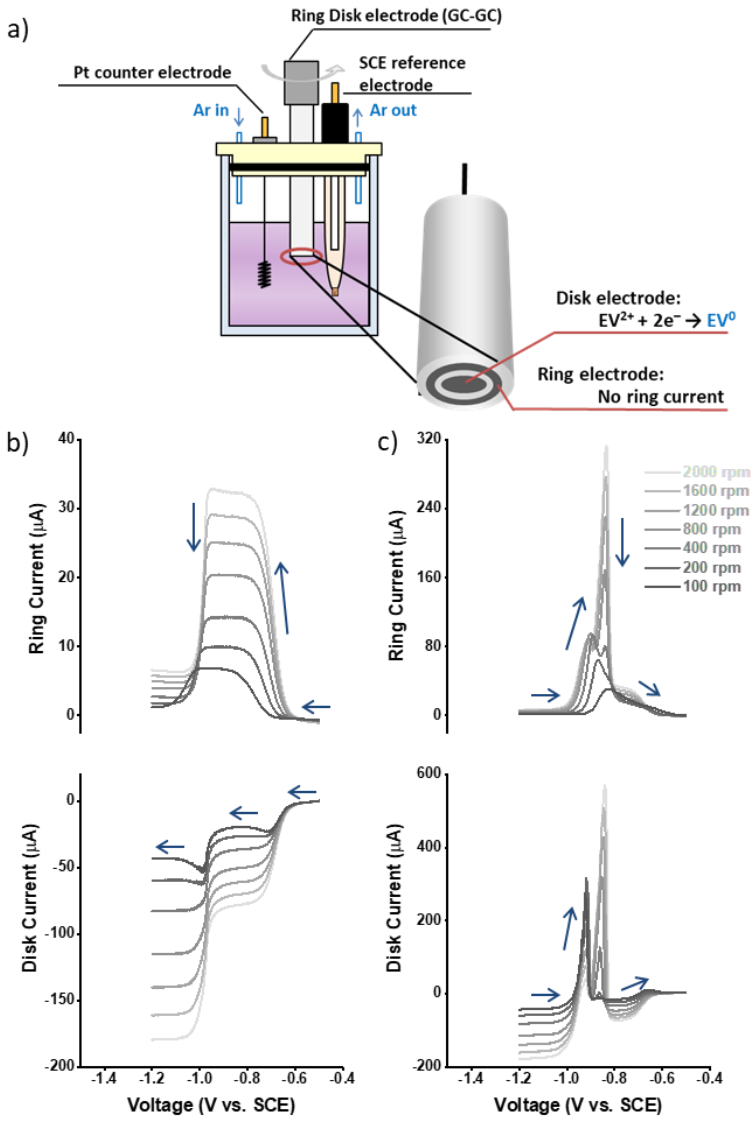

Fig. S11 (a) The schematic representation of the RRDE test of EV when the disk potential is lower than – 1.0 V vs. SCE. RRDE of 1 mM EV in 0.5 M NaCl aqueous electrolyte during (b) the negative-going scan and (c) the positive-going scan. Ring and disk currents were recorded at 50 mV s^{-1} with rotation rates between 100 and 2000 rpm and continuously holding the GC ring electrode at − 0.5 V vs. SCE.

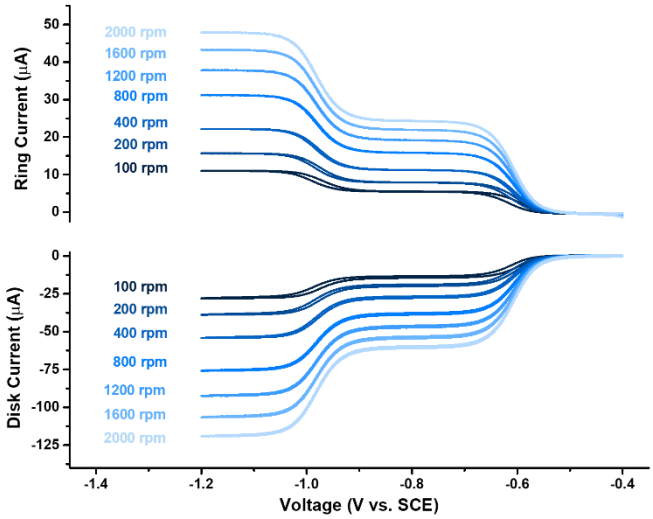

Fig. S12 RRDE of 1 mM Vi-OEG3 in 0.5 M NaCl aqueous electrolyte. Ring and disk currents were recorded at 5 mV s^{-1} with rotation rates between 100 and 2000 rpm and continuously holding the GC ring electrode at − 0.4 V vs. SCE.

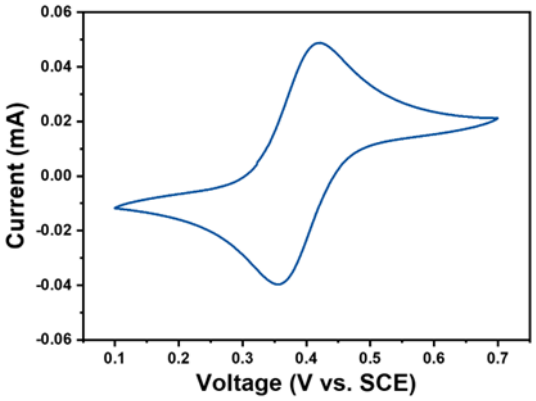

Fig. S13 CV of FcNEBr. Condition: 5 mM FcNEBr in 0.5 M NaBr aqueous electrolyte at a scan rate of 50 mV s^{-1}.

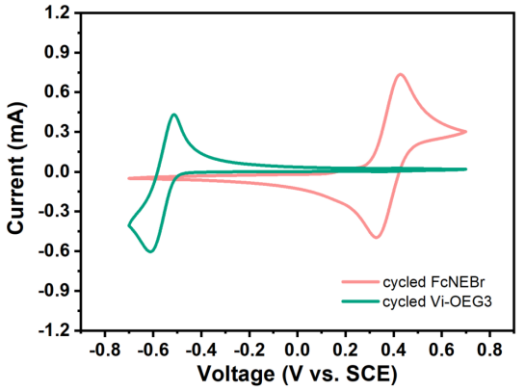

Fig. S14 CV of electrolytes after cycling (0.5 M flow cell in Fig. 4).

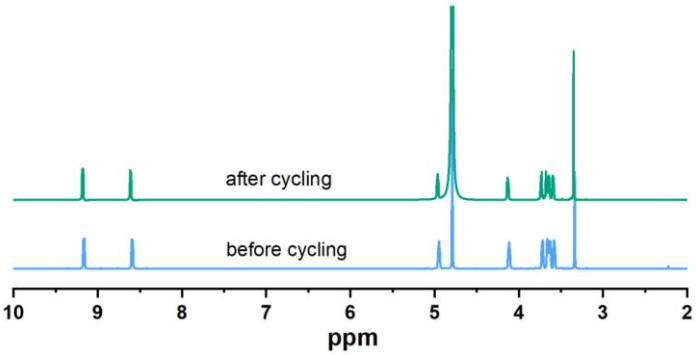

Fig. S15 ^{1}H NMR of Vi-OEG3 negolytes before and after cycling (0.5 M flow cell in Fig. 4).

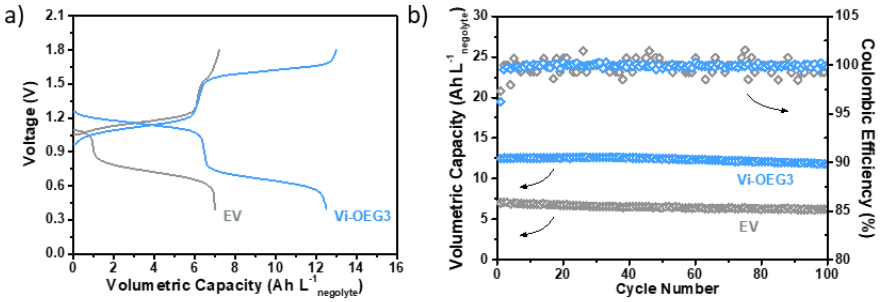

Fig. S16 (a) Galvanostatic voltage profile of 0.25 M EV/0.5 M FcNEBr and 0.25 M Vi-OEG3/0.5 M FcNEBr static cell (1st cycle). (b) Cycling retention of volumetric capacity and coulombic efficiency of 0.25 M EV/0.5 M FcNEBr and 0.25 M Vi-OEG3/0.5 M FcNEBr static cell. Posolyte: 0.5 M FcNEBr in 1 M NaBr supporting electrolyte; Negolyte: 0.25 M EV or Vi-OEG3 in 1 M NaBr supporting electrolyte.

Table S1. Summary of state-of-the-art representative viologen-based AORFBs.

electrolyte		volume (mL)		cycling stability		E/P (h)[a]	ref.
posolyte	negolyte	posolyte	negolyte	time (days)	number		
0.5 M TMAP-TEMPO in 1 M NaCl	0.5 M BTMAP-Vi in 1 M NaCl	10	15	~ 3.4	200	0.2	[2]
1.5 M TMAP-TEMPO in 4.5 M NaCl	1.5 M BTMAP-Vi	5	7.5	~ 7.2	250	0.34	
2 M FcNCl	2M BHOP-Vi	10	5	~ 4.8	100	0.57	[3]
0.5 M $(NH_4)_4[Fe(CN)_6]$	0.5 M $(SPr)_2V$ in 1.0 M NH_4Cl	12	12	~ 4.6	300	0.18	[4]
2.0 M KI in 2.0 M KCl	0.5 M $(SPr)_2V$ in 2.0 M KCl	12	12	~ 4.6	300	0.18	
0.3 M $K_4Fe(CN)_6$ + 0.3 M $K_3Fe(CN)_6$ in 2 m NH_4Cl at pH = 9	1.0 M BPP-Vi titrated with 14 m NH_4OH to pH = 9	40	6.2	~ 13	280	0.56	[5]
0.1 M BTMAP-Fc	0.1 M Dex-Vi in 1 M NaCl	10	5.5	~ 14	1200	0.14	[6]
0.75 M BTMAP-Fc	1.5 M Dex-Vi	15	5	~ 30	340	1.05	
0.5 M FcNCl + 1 M NaCl	0.5 M BTMAE-Vi in 1 M NaCl	10	5	~ 1.6	200	0.1	[7]
0.4 M FcNEBr + 1 M NaBr	**0.5 M Vi-OEG3 + 1 M NaBr**	**10**	**5**	**~ 6**	**138**	**0.52**	**This work**

[a] E/P represents the energy-to-power ratio, which is the discharge time duration of each cycle.

References

1. W. Wang, N.-C. Lai, Z. Liang, Y. Wang and Y.-C. Lu, *Angewandte Chemie International Edition*, 2018, **57**, 5042-5046.
2. Y. Liu, M.-A. Goulet, L. Tong, Y. Liu, Y. Ji, L. Wu, R. G. Gordon, M. J. Aziz, Z. Yang and T. Xu, *Chem*, 2019, **5**, 1861-1870.
3. Y. Liu, Y. Li, P. Zuo, Q. Chen, G. Tang, P. Sun, Z. Yang and T. Xu, *ChemSusChem*, 2020, **13**, 2245-2249.
4. C. DeBruler, B. Hu, J. Moss, J. Luo and T. L. Liu, *ACS Energy Letters*, 2018, **3**, 663-668.
5. S. Jin, E. M. Fell, L. Vina-Lopez, Y. Jing, P. W. Michalak, R. G. Gordon and M. J. Aziz, *Advanced Energy Materials*, 2020, **10**, 2000100.
6. X.-L. Lv, P. Sullivan, H.-C. Fu, X. Hu, H. Liu, S. Jin, W. Li and D. Feng, *ACS Energy Letters*, 2022, **7**, 2428-2434.
7. K. Peng, P. Sun, Z. Yang and T. Xu, *Batteries & Supercaps*, 2023, **6**, e202200426.